Structural and Thermal Properties of Tetragonal Double Tungstate Crystals Intended for Ytterbium Laser Composites

Xiumei Han, Alberto García-Cortés, María Dolores Serrano, Carlos Zaldo, and Concepción Cascales*

Instituto de Ciencia de Materiales de Madrid, Consejo Superior de Investigaciones Científicas, c/Sor Juana Inés de la Cruz, 3, E-28049 Madrid, Spain

Crystals of undoped and laser active Yb-doped $NaT_{1-x}Yb_x(WO_4)_2$, T = Y (x = 0, 0.1), Lu (x = 0, 0.1, 0.5), have been grown by the Czochralski (T = Y) or the top seeded solution growth (T = Lu) methods, depending on their melting nature, congruent or incongruent, respectively. From single-crystal X-ray diffraction analysis, the noncentrosymmetric tetragonal space group $I\bar{4}$ has been established for all of them. The Na^+/T^{3+} (Yb^{3+}) occupancy factors for $2b$ and $2d$ sites show the lowest departure from the random distribution, and thus the largest cationic disorder, in $NaLu_{0.9}Yb_{0.1}(WO_4)_2$, namely 0.43/0.57 and 0.56/0.44, respectively. The thermal expansion tensors have been determined up to 973 K for the five crystals; $NaLu(WO_4)_2$ with α_1=8.2(2) $\times$ 10^{-6} K^{-1} and α_3= 17.3(4) $\times$ 10^{-6} K^{-1} coefficients has lower anisotropy than $NaY(WO_4)_2$ with α_1= 8.4(2) $\times$ 10^{-6} K^{-1} and α_3=18.5(4) $\times$ 10^{-6} K^{-1} coefficients. From the point of view of the thermal steadiness, the evaluation of the Yb-doped laser layer/optically inert substrate lattice mismatch, about 2.5 times higher for $NaY_{0.9}Yb_{0.1}(WO_4)_2/NY(WO_4)_2$ than for $NaLu_{0.9}Yb_{0.1}(WO_4)_2/NaLu(WO_4)_2$ at temperatures up to 973 K, points out to this last set as the best simple combination of tetragonal Na-based double tungstates intended for epitaxially grown laser active composites. An approach to minimize the laser layer/substrate lattice mismatch derived of the Yb incorporation in the layer is developed through the tailoring of the composition of its optically inert substrate.

Introduction

The use of infrared diode lasers for optical pumping in the present solid-state laser technology turns the growth of Yb^{3+}-doped crystalline laser hosts into an issue of major interest. Yb^{3+} with strong absorption at about 980 nm can be pumped by the robust InGaAs lasers, and it is used for the emission at 1.05 μm,[1] or as sensitizer of Er^{3+} and Ho^{3+}, for emissions at 1.5 and 2 μm, respectively.[2] The $^2F_{5/2} \rightarrow$ $^2F_{7/2}$ Yb^{3+} laser emission at 1.05 μm is an advantageous alternative to the $^4F_{3/2} \rightarrow$ $^4I_{11/2}$ Nd^{3+} one at 1.06 μm: (i) The lower quantum defect of Yb^{3+} in comparison to Nd^{3+} helps to control the host thermal lensing, although hosts with high thermal conductivity or cooling systems are still needed to minimize the electron population of the terminal Stark sublevel in the three-level Yb^{3+} laser. (ii) The absence of energy levels above the Yb^{3+} $^2F_{5/2}$ excited state avoids detrimental losses by up-conversion. (iii) The upper state Yb^{3+} $^2F_{5/2}$ lifetime is about 3 times longer than the Nd^{3+} $^4F_{3/2}$ lifetime in a considered host, leading to lower pump threshold intensity, and improving energy storage for Q switching. (iv) For a given medium, Yb^{3+} has smaller fluorescence quenching than Nd^{3+}, which allows the incorporation of higher Yb^{3+} dopant levels without degradation of the radiative properties.

All these Yb^{3+} advantages are of particular interest for the thin disk laser technology, which uses as active laser medium disks with thickness <200 μm attached to a heat sink.[3] Such thin laser disks are mechanically fragile and difficult to handle. To enhance their strength they can be prepared as layers onto thicker ($\approx$1 mm) isostructural optically inert crystals, i.e., composite laser crystals,[4] with various additional benefits: the reduction of the beam quality requirements for the pump source, the reduction of the trend for transverse amplified spontaneous emission and parasitic lasing in large disks, and a possible improvement of the cooling. Another possible application of Yb-doped layers is the production of laser waveguides based on the increase of the refractive index with Yb doping.[5] In fact, Yb-doping increases the extraordinary refractive index of $NaGd(WO_4)_2$,[6] and therefore, this application seems feasible for some tetragonal double tungstate composites.

The laser performance of these composites is strongly influenced by the presence of light scattering defects originating at the layer/substrate interface and propagating into

(3) Giesen, A. *Laser Technik J.* **2005**, *2*, 42.
(4) Zapata, L.; Beach, R.; Payne, S. *Composite Thin-Disk Laser Scaleable to 100 kW Average Power Output and Beyond*; Preprint UCRL-JC-138786; Lawrence Livermore National Laboratory, 2000.
(5) Romanyuk, Y. E.; Borca, C. N.; Pollnau, M.; Rivier, S.; Petrov, V.; Griebner, U. *Opt. Lett.* **2006**, *31*, 53.
(6) Cascales, C.; Serrano, M. D.; Esteban-Betegón, F.; Zaldo, C.; Peters, R.; Petermann, K.; Huber, G.; Ackermann, L.; Rytz, D.; Dupré, C.; Rico, M.; Liu, J.; Griebner, U.; Petrov, V. *Phys. Rev. B* **2006**, *74*, 174114.

* To whom correspondence should be addressed. E-mail ccascales@icmm.csic.es.

(1) Krupke, W. F. *IEEE J. Sel. Top. Quantum Electron.* **2000**, *6*, 1287.
(2) Scheps, R. *Prog. Quantum Electron.* **1996**, *20*, 27.

the laser layer bulk. Hence, a very low lattice mismatch between the doped layer and the optically inert substrate is required to grow free-of-defect epitaxial composites. Isostructural, optically inert Y^{3+}- and Lu^{3+}-based crystal hosts are the choice substrates to grow Yb^{3+}-doped laser active layers[7,8] due to the closeness of ionic radii sizes, 1.019, 0.977, and 0.985 Å, for Y^{3+}, Lu^{3+}, and Yb^{3+} cations, respectively.[9]

The thin disk laser concept has been applied very successfully to extract high power laser intensities[10] and to achieve tunable lasers.[11] The laser active material for demonstration of tunability in thin disks was Yb-doped YAG, with a relatively narrow tuning range, ≈35 nm around 1030 nm.

Disordered Yb-doped bulk crystals with inhomogeneously broadened bands have shown their capability for extended laser tunable response. A wide class of these disordered materials are the tetragonal double tungstates (DTs) with nominal formula $MT(WO_4)_2$, where M is a monovalent cation, like the alkaline ones and Ag, and T is a trivalent cation, including Bi, Y, La, and all lanthanides. We shall refer to these crystals as MTW. Over the last 2 years, CW tunable laser operation has been shown in Yb-doped NaYW,[12] NaLaW,[13] NaGdW,[6,14] and NaLuW[15] crystals as well as in other isostructural double molybdates (DMs) like $NaLa(MoO_4)_2$[16] and $LiGd(MoO_4)_2$.[17] Despite the limited spectral response of the optical cavities used, the tunability of these lasers extended up to 65 nm, 1014−1079 nm.[6] When the total Yb^{3+} bandwidth is considered, these Yb-doped DT crystals are potential candidates to support <50 fs laser pulses by mode-locking laser operation. In fact, 53 fs pulses have been already demonstrated using bulk crystals.[12] Therefore, tetragonal DTs are candidates for thin disk laser technology, and composites with suitable Yb doping will be required.

In Na-based DT crystals solidified from their melts, it has been observed that above a certain Yb concentration, typically 15 mol % for NaLaW[18] and 20 mol % for NaGdW,[6]

micrometer-size bubbles appear. For higher Yb concentrations even the crystal seeding was not possible. This behavior has to do with the melting nature of NaTWcompounds, which is congruent for T = La−Er, while for T = Tm, Yb, and Lu is incongruent.[19] Therefore, in the first case single crystals can be grown by the Czochralski (Cz) method, and for the second series the top seeded solution growth (TSSG) method using a flux, either Na_2WO_4 or $Na_2W_2O_7$, is needed to keep the compounds below their decomposition temperature. Independent of the substrate, the growth of the active $NaT_{1-x}Yb_xW(T = Y$ or Lu) layer by liquid-phase epitaxy would require the use of a flux at high temperature, typically ≈1200 K. Defects can be generated at the growth stage to accommodate the different layer and substrate lattice parameters. Further defects can be created upon cooling to room temperature to release the stress associated with the different layer and substrate thermal properties. No detailed information on these aspects is available for tetragonal DTs of interest for composites.

Although some preliminary crystallographic information on polycrystalline samples of NaYbW[19−21] and NaLuW[22] is available, single-crystal X-ray structure data exists neither for NaYW and NaLuW, nor for their Yb-doped analogues. On the other hand, the preparation method of the NaYbW sample of ref 21 is unidentified, and the reported unit cell parameters at 300 K, $a = 5.3309$ Å, $c = 11.6669$ Å, are considerably larger than those previously determined, $a = 5.18$ Å, $c = 11.19$ Å,[19] and $a = 5.175$ Å, $c = 11.190$ Å.[20] $NaLu(WO_4)_2$ crystals in ref 22 were grown using a sodium bitungstate flux, but the crystal structure information provided is limited to the 300 K unit cell parameters determined from the powdered sample, $a = 5.166$ Å, $c = 11.174$ Å. In the mentioned studies, the tetragonal centrosymmetric space group (SG) $I4_1/a$ (No. 88) was established. More recently, the presence of a few non-negligible (006, 00$\bar{6}$, 002, $\bar{1}$10, and 1$\bar{1}$0) Bragg reflections in NaGdW,[6] NaBiW,[23,24] NaBiMo,[24,25] and LiBiMo[24] led to their description in the more adequate noncentrosymmetric SG $I\bar{4}$ (No. 82), even if for NaBiW and NaBiMo a re-evaluation of the crystal symmetry yielded again the SG $I4_1/a$.[26,27] Anyway, these uncertainties may derive from the possible nonstoichiometric composition of some of the crystals, which have been grown under different conditions, and from the different experimental procedures followed for structural studies.

(7) Ubizskii, S. B.; Matkovskii, A. O.; Melnyk, S. S.; Syvorotka, I. M; Müller, V.; Peters, V.; Petermann, K.; Beyertt, A.; Giesen, A. *Phys. Status Solidi A* **2004**, *201*, 791.
(8) Griebner, U.; Liu, J.; Rivier, S.; Aznar, A.; Grunwald, R.; Solé, R. M.; Aguiló, M.; Díaz, F.; Petrov, V. *IEEE J. Quantum Electron.* **2005**, *41*, 408.
(9) Shannon, R. D. *Acta Crystallogr., Sect. A* **1976**, *32*, 751.
(10) Stewen, C.; Contag, K.; Larionov, M, Giesen, A.; Hügel, H. *IEEE J. Sel. Top. Quantum Electron.* **2000**, *6*, 650.
(11) Brauch, U.; Giesen, A.; Karszewski, M.; Stewen, C.; Voss, A. *Opt. Lett.* **1995**, *20*, 713.
(12) García-Cortés, A.; Cano-Torres, J. M.; Serrano, M. D.; Cascales, C.; Zaldo, C.; Rivier, S.; Mateos, X.; Griebner, U.; Petrov, V. *IEEE J. Quantum Electron.,* submitted.
(13) Liu, J.; Cano-Torres, J. M.; Cascales, C.; Esteban-Betegón, F.; Serrano, M. D.; Volkov, V.; Zaldo, C.; Rico, M.; Griebner, U.; Petrov, V. *Phys. Status Solidi A* **2005**, *202*, R29.
(14) Rico, M.; Liu, J.; Griebner, U.; Petrov, V.; Serrano, M. D.; Esteban-Betegón, F.; Cascales, C.; Zaldo, C. *Opt. Express* **2004**, *12*, 5362.
(15) García-Cortés, A.; Cano-Torres, J. M.; Han, X.; Cascales, C.; Zaldo, C.; Mateos, X.; Rivier, S.; Griebner, U.; Petrov, V.; Valle, F. J. *J. Appl. Phys.* **2007**, *101*, 063110.
(16) Rico, M.; Liu, J.; Cano-Torres, J. M.; García-Cortés, A.; Cascales, C.; Zaldo, C.; Griebner, U.; Petrov, V. *Appl. Phys. B* **2005**, *81*, 621.
(17) Rico, M.; Griebner, U.; Petrov, V.; Ortega, P.; Han, X.; Cascales, C.; Zaldo, C. *J. Opt. Soc. Am. B* **2006**, *23*, 1083.
(18) Serrano, M. D.; Esteban-Betegón, F.; Zaldo, C. *J. Cryst. Growth* **2005**, *275*, e819.

(19) Rode, E. Ya.; Karpov, V. N.; Ivanova, M. M.; *Russ. J. Inorg. Chem. (Engl. Transl.)* **1971**, *6*, 905; *Zh. Neorg. Khim.* **1971**, *16*, 1713.
(20) JCPDS-ICDD file 25-0887.
(21) Sadanandam, J.; Suryanarayana S. V. *Natl. Acad. Sci. Lett. (India)* **1979**, *2*, 195.
(22) Klevtsova, R. F.; Glinskaya, L. A.; Kozeeva, L. P.; Klevtsov, P. V. *Sov. Phys. Crystallogr.* **1973**, *17*, 672.
(23) Hanuza, J.; Benzar, A.; Haznar, A.; Maczka, M.; Pietraszko, A.; van der Maas, J. H. *Vib. Spectrosc.* **1996**, *12*, 25.
(24) Rico, M.; Méndez-Blas, A.; Volkov, V.; Monge, M. A.; Cascales, C.; Zaldo, C.; Kling, A.; Fernández-Díaz, M. T. *J. Opt. Soc. Am. B* **2006**, *23*, 2066.
(25) Hanuza, J.; Haznar, A.; Maczka, M.; Pietraszko, A.; Lemiec, A.; van der Maas, J. H.; Lutz, E. T. G. *J. Raman Spectrosc.* **1997**, *28*, 953.
(26) Wáskowska, A.; Gerward, L.; Staun Olsen, J.; Maczka, M.; Lis, T.; Pietraszko, A.; Morgenroth, W. *J. Solid State Chem.* **2005**, *178*, 2218.
(27) Maczka, M.; Kokanyan, E. P.; Hanuza, J. *J. Raman Spectrosc.* **2005**, *36*, 33.

Table 1. Growth Conditions and Composition of Cz and TSSG NaT$_{1-x}$Yb$_x$(WO$_4$)$_2$ Crystals

		Czochralski Grown NaY$_{1-x}$Yb$_x$(WO$_4$)$_2$		
melting temperature (K)	[Yb]$_{MELT}$ (mol %)		[Yb]$_{CRYSTAL}$ (10^{20} cm^{-3})	XRFS composition
1483	0			Na$_{0.935}$Y$_{1.046}$W$_{1.988}$
1475	10		4.52	Na$_{0.963}$Y$_{0.965}$Yb$_{0.069}$W$_{1.99}$

		Top Seeded Solution Grown NaLu$_{1-x}$Yb$_x$(WO$_4$)$_2$			
solute:flux (molar ratio)	cooling interval (K)	cooling rate (K/h)	[Yb]$_{MELT}$ (mol %)	[Yb]$_{CRYSTAL}$ (10^{20} cm^{-3})	XRFS composition
1:4	1150−1118	0.03	≈0	0.38	Na$_{1.011}$Lu$_{0.997}$Yb$_{0.006}$W$_{1.988}$[a]
1:6	1107−1097	0.02	10	7.46	Na$_{1.027}$Lu$_{0.874}$Yb$_{0.111}$W$_{2.002}$
1:3.5	1190−1176	0.04	50	34.0	Na$_{1.014}$Lu$_{0.481}$Yb$_{0.508}$W$_{2.002}$

[a] The Yb doping for this crystal was unintentional.

Table 2. Crystal Data at 296(2) K and Refinement Details for NaT$_{1-x}$Yb$_x$(WO$_4$)$_2$[a]

	NaYW	NaY$_{0.9}$Yb$_{0.1}$W	NaLuW	NaLu$_{0.9}$Yb$_{0.1}$W	NaLu$_{0.5}$Yb$_{0.5}$
Mo Kα radiation λ (Å)	0.71073	0.71073	0.71073	0.71073	0.71073
cryst syst, space group	tetragonal, $I\bar{4}$ (No. 82)	tetragonal, $I\bar{4}$ (No. 82)	tetragonal, $I\bar{4}$ (No. 82)	tetragonal, $I\bar{4}$ (No. 82)	tetragonal, $I\bar{4}$ (No. 82)
unit cell dimensions (Å)					
a	5.2014(4)	5.2018(8)	5.1692(3)	5.1702(11)	5.1715(7)
c	11.2740(12)	11.2719(25)	11.1832(15)	11.179(4)	11.190(2)
V (Å^3)	305.01(5)	305.00(8)	298.82(5)	298.83(13)	299.26(8)
Z	2	2	2	2	2
calcd density (Mg/m^3)	6.616	6.616	7.709	7.709	7.687
abs coeff (mm^{-1})	47.130	47.126	54.866	54.864	54.351
$F(000)$	524	524	588	588	587
cryst size (mm^3)	0.2 × 0.1 × 0.1	0.15 × 0.09 × 0.05	0.2 × 0.12 × 0.07	0.15 × 0.1 × 0.08	0.2 × 0.12 × 0.1
θ range of data collection (deg)	3.61−33.02	3.62−28.99	3.64−30.44	3.65−33.04	3.64−27.88
hkl limiting indices					
h	−7 to 4	−7 to 3	−5 to 6	−7 to 4	−3 to 5
k	−6 to 7	−4 to 7	−7 to 3	−4 to 7	−6 to 6
l	−15 to 5	−14 to 13	−15 to 12	−15 to 12	−14 to 14
reflns collected/unique	786/453	648/316	727/405	754/446	725/309
R_{int}	0.0297	0.0486	0.0258	0.0512	0.0298
refinement method	full-matrix least-squares on F^2	full-matrix least-squares on F^2	full-matrix least-squares on F^2	full-matrix least-squares on F^2	full-matrix least-squares on F^2
data/restraints/params	453/2/32	316/2/34	405/2/34	446/2/22	309/2/34
GOF on F^2	1.117	0.996	1.075	1.013	1.217
final R indices [$I > 2\sigma(I)$] R1, wR2	0.0567, 0.1486	0.0599, 0.1959	0.0617, 0.1698	0.0570, 0.1523	0.0439, 0.1385
R indices (all data) R1, wR2	0.0657, 0.1689	0.0655, 0.2028	0.0657, 0.1761	0.0695, 0.1641	0.0511, 0.1537
extinction coeff	0.019(3)	0.035(11)	0.09(2)	0.10(2)	0.027(7)
systematic absence exceptions					
hkl I > 3σ for 4$_1$ axis	2	1	3	1	3
(total *hkl I* > 2σ)	(3)	(2)	(5)	(3)	(7)
hkl I > 3σ for *a* plane	8	3	3	2	10
(total *hkl I* > 2σ)	(16)	(14)	(14)	(11)	(18)

[a] T = Y or Lu.

The purpose of the present work is to provide the crystallographic information required to select the most suited Yb-doped layer and optically inert substrate combination, in terms of the preparation procedures, low defect density, and physical characteristics. Hence, we carried out a comprehensive single-crystal X-ray diffraction study of the structure of NaYW, NaLuW, and NaT$_{1-x}$Yb$_x$W (T = Y or Lu) grown crystals, with particular emphasis on determining the distribution of Na$^+$ and Y^{3+}/Yb^{3+}/Lu^{3+} cations over the point sites that they occupy in the lattice. Compositional and crystallographic differences associated with the used growth method, either Cz or TSSG, are discussed. The crystallochemical properties of these systems are also compared to those reported for NaGdW and Yb^{3+}-doped NaGdW crystals.[6] To predict the thermal evolution of NaT$_{1-x}$Yb$_x$W/NaTW (T = Y or Lu) composites during the growth and cooling steps of their preparation as well as under heating induced by the optical pumping, we evaluated the thermal expansion tensors α$_{ij}$ of the corresponding pure and Yb-doped crystals. Finally, we discuss an approach to achieve zero lattice-mismatch in Yb-doped layer/inert substrate composites of tetragonal DTs, based on tailoring the layer and substrate compositions.

Experimental Section

Crystal Growth and Preparation of Polycrystalline Samples. Crystal growth experiments were made using 75 cm^3 Pt-crucibles and vertical tubular furnaces with SiC (Cz growth method) or Kantal-A1 (TSSG method) heating elements. The temperature was set with stability better than ±0.2 °C using Eurotherm 808 temperature controllers. Undoped and Yb-doped NaYW crystals were grown by the Cz method, in air, following procedures previously described for other tetragonal NaTW crystals.[6,28] We used WO$_3$ (99.998% Alfa Aesar), Na$_2$CO$_3$ (99.997% Alfa Aesar), Y$_2$O$_3$ (99.99% Alfa Aesar), and Yb$_2$O$_3$ (99.99% Alfa Aesar) as starting reagents. Despite the congruent melt of NaYW (mp 1483 K), an excess of 2.3 mol % of Na$_2$W$_2$O$_7$ (mp 1005 K) was added

(28) García-Cortés, A.; Cascales, C.; de Andrés, A.; Zaldo, C.; Zharikov, E. V.; Subbotin, K. A.; Bjurshagen, S.; Pasiskevicius, V.; Rico, M. *IEEE J. Quantum Electron.* **2007**, *43*, 157.

to decrease the growing temperature, which eases the seeding process and partially compensates Na and W volatilities from the melt.

Crystals of $NaLu_{1-x}Yb_xW$ were grown by the TSSG method using $Na_2W_2O_7$ flux. Yb-doping levels in the melt of 10 mol %, similar to its concentrations in other isostructural laser Na−DT crystals,[6,13,14] and 50 mol %, to explore the features of a high level of Yb in the crystal, were chosen. Required amounts of WO_3 (99.8% Aldrich), Na_2CO_3 (99.5% Alfa Aesar), Yb_2O_3 (99.9% Alfa Aesar), and Lu_2O_3 (99.99% purchased through Shanghai Zimei International Trade Co LTD) were used to synthesize the $NaLu_{1-x}Yb_xW$ (solute) and $Na_2W_2O_7$ (flux) polycrystalline phases. Solute/flux mixtures, in the ratios indicated in Table 1, were held for several days at ≈50 K above their melting temperature. Pt wire and *c*-cut NaGdW crystals were used as seeds. The seed rotation and the cooling rates were in 10−30 rpm and 0.02−0.04 K/h ranges, respectively.

The crystal composition was determined by X-ray fluorescence spectrometry (XRFS), using specifically developed standards in which the reagents were melted in $Li_2B_4O_7$ forming a disk. The calibration procedure allows for perfect reproducibility in the standards of the X-ray reabsorption in the analyzed samples. The weight of the compounds was controlled with a resolution of 5×10^{-5} g. For each element, a preliminary study allowed the selection of the X-ray emission free of spectral overlaps with emissions from other elements, or alternatively to take into account these contributions. Following these procedures the uncertainty of the molar concentrations determined is lower than ±0.002. This high accuracy is reflected in the determined low concentration of Yb in the nominally undoped NaLuW crystal, see Table 1.

Series of polycrystalline $NaLu_{1-x}T_xW$ samples with compositions T = La (*x* = 0.03, 0.06, 0.10, 0.15), Gd, or Y (*x* = 0.05, 0.10, 1.015, 0.20, 0.25) were prepared from the same reagents, by annealing in air up to 1326 K over 120 h. The purity of the required tetragonal phase was, in each case, tested by 300 K XRPD with a Bruker AXS D-8 Advance diffractometer, using Cu Kα radiation.

X-ray Single-Crystal Structure Determination. X-ray diffraction analyses of undoped NaTW and $NaT_{1-x}Yb_xW$ (T = Y or Lu) crystals have been performed from data collected at room temperature with a Bruker SMART CCD diffractometer equipped with a normal focus 3 kW sealed tube. Small single crystals cut from each grown material were selected in order to minimize the possibility of twinning. Data were collected over a quadrant of the reciprocal space by a combination of three sets of exposures. Each set had a different φ angle for the crystal, and each exposure of 20 s covered 0.3° in ω. The crystal-to-detector distance was 4.99 cm. For each crystal, the unit cell parameters were initially determined by a least-square fit of about 30 reflections with $I > 20\sigma(I)$. Neutral-atom scattering factors for all atoms were used, and anomalous dispersion corrections were applied.[29] The calculations have been performed using the SHELXTL program,[30] and the views of the structure have been drawn with the ATOMS software.[31]

High-Temperature X-ray Powder Diffraction Analysis. Thermal expansion coefficients were calculated from XRPD above 300 K made in air on ground crystals. XRPD data were collected using a Panalytical X'Pert PRO MPD diffractometer system, with a PW3050/60 goniometer in $\theta-\theta$ scan configuration and an X'Celerator detector, equipped with an Anton Paar HTK-1200 high-temperature chamber. Monochromatic Cu Kα_1 radiation ($\lambda =$
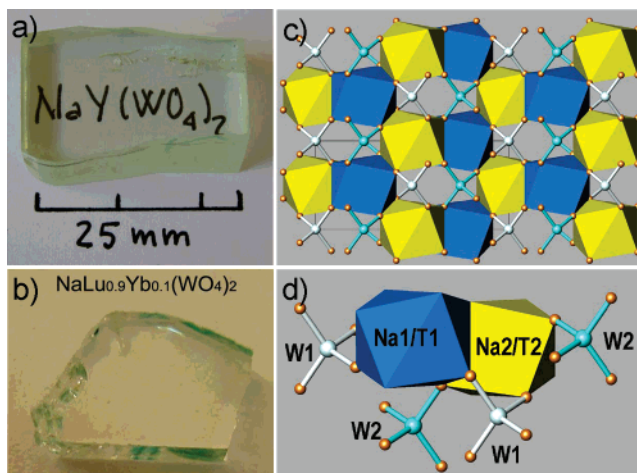

Figure 1. (a) Polished $NaY(WO_4)_2$ (Cz-grown) and (b) $NaLu_{0.90}Yb_{0.10}$-$(WO_4)_2$ (TSSG) plates. (c) *ac*-Projection of the tetragonal $I\bar{4}$ crystal structure of $NaT(WO_4)_2$, showing $(Na/T)O_8$ polyhedra from the $2d(1)$ and $2b(2)$ positions and the two kinds of WO_4 tetrahedra. (d) Detail of the edge-sharing $(Na/T)_2O_{14}$ dimeric units and WO_4 tetrahedra.

1.540560 Å) from a PW3373/00 X-ray tube was used, and the generator was set to 45 kV and 40 mA. The samples were disposed in alumina holder disks. The X-ray patterns were recorded over the 2θ range between 15° and 70°, in continuous scan mode with angular step size of 0.01675° and a counting step time of 2 s, at temperatures of 303, 323, 348, 373, 398, 423, 448, 473, 523, 573, 673, 723, 773, 873, and 973 K. This range of temperature is large enough to adequately describe the behavior of crystals under cooling from the growth temperature and under heating during optical pumping.

Since XRPD data are not sufficient to support an unambiguous complete crystal structure determination from a Rietveld refinement, due to the large number of parameters required and also to the presence of preferred orientation in these pulverized crystals, the following procedure was used to avoid errors in the determination of unit cell parameters. Data sets of ≈30 experimentally observed *hkl* reflections at each temperature were indexed with the symmetry of the space group $I\bar{4}$. For this indexing purpose, simulations of the room-temperature Rietveld pattern profiles of the five NaTW and $NaT_{1-x}Yb_xW$ (T = Y or Lu) samples were carried out with the WinPLOTR program,[32] using the crystallographic data derived from the corresponding previous X-ray single-crystal structure determination, in order to compare the Bragg reflections with those observed in experimental XRPD patterns. The lattice parameters were then calculated and refined by the least-squares method using the entire sets of experimental reflections at each temperature.

Results and Discussion

Crystal Growth and Composition Results. Cz-grown crystals with sizes up to 30 mm long and 25 mm in diameter were obtained, while crystals grown by the TSSG method were limited to less than $10 \times 10 \times 10$ mm³. Figure 1a,b shows polished NaYW and $NaLu_{0.9}Yb_{0.1}W$ crystal plates. It is worth noting than the highly Yb-doped $NaLu_{0.5}Yb_{0.5}W$ crystal was transparent and free of macrodefects.

The melting temperature of the $Na_2W_2O_7$-enriched $NaY_{1-x}Yb_xW$ composition decreases slightly with increasing Yb concentration, whereas the observed decrease in the

(29) *International Tables for Crystallography*; Kynoch Press: Birmingham, U.K., 1974; Vol. 4.

(30) *SHELXTL Version 6.10 software package*; Siemens Energy and Automation Inc. Analytical Instrumentation.

(31) Dowty, E. *ATOMS v. 5.1, Computer Program for Displaying Atomic Structures*; Kingsport, TN, 2001.

(32) Roisnel, T.; Rodriguez Carvajal, J. *WinPLOTR*; plotr@llb.saclay.cea.fr, http://www.-llb.cea.fr/fullweb/winplotr/winplotr.htm.

Table 3. Atomic Coordinates ($\times 10^4$) and Equivalent Isotropic Displacement Parameters ($\text{Å}^2 \times 10^3$) for $\text{NaT}_{1-x}\text{Yb}_x(\text{WO}_4)_2$, T = Y or Lu, Crystals

			NaYW	$\text{NaY}_{0.9}\text{Yb}_{0.1}\text{W}$	NaLuW	$\text{NaLu}_{0.9}\text{Yb}_{0.1}\text{W}$	$\text{NaLu}_{0.5}\text{Yb}_{0.5}\text{W}$
Na(1)/T(1)	2d	x, y, z			$^1/_2, 0, ^1/_4$		
		$U(\text{eq})^a$	10(8)	17(5)	8(4)	6(6)	7(3)
		OF^b	0.67(1)/0.33(1)	0.67(1)/0.33(1)	0.57(1)/0.43(1)	0.56(1)/0.44(1)	0.59(2)/0.42(4)
Na(2)/T(2)	2b	x, y, z			$^1/_2, ^1/_2, 0$		
		$U(\text{eq})$	14(6)	7(6)	8(5)	7(4)	10(2)
		OF	0.26(1)/0.74(1)	0.26(1)/0.74(1)	0.42(1)/0.58(1)	0.43(1)/0.57(1)	0.40(2)/0.59(4)
W(1)	2a	x, y, z			0, 0, 0		
		$U(\text{eq})$	8(1)	26(4)	8(3)	5(4)	8(2)
		OF	1.00	0.92(5)	0.95(2)	1.00(3)	1.00
W(2)	2c	x, y, z			$0, ^1/_2, ^1/_4$		
		$U(\text{eq})$	11(2)	9(1)	8(2)	4(3)	10(2)
		OF	1.00	0.93(4)	0.97(2)	0.98(2)	1.00
O(1)	8g	x	2390(30)	2420(40)	2380(30)	2420(50)	2440(30)
		y	8480(30)	8360(40)	8450(30)	8410(50)	8460(20)
		z	845(14)	850(20)	870(13)	870(20)	852(12)
		$U(\text{eq})$	17(3)	17(6)	20(5)	17(7)	18(4)
O(2)	8g	x	2460(40)	2450(60)	2440(30)	2510(50)	2450(30)
		y	3410(30)	3530(50)	3380(30)	3390(50)	3380(30)
		z	1643(14)	1660(30)	1633(13)	1640(20)	1641(13)
		$U(\text{eq})$	18(3)	35(7)	12(5)	18(7)	19(4)
X-ray refined composition			$\text{Na}_{0.93}\text{T}_{1.07}\text{W}_2$	$\text{Na}_{0.93}\text{T}_{1.07}\text{W}_{1.85}$	$\text{Na}_{0.99}\text{T}_{1.01}\text{W}_{1.92}$	$\text{Na}_{0.99}\text{T}_{1.01}\text{W}_{1.98}$	$\text{Na}_{0.99}\text{T}_{1.01}\text{W}_2$

^{a} U(eq) is defined as one-third of the trace of the orthogonalized U^{ij} tensor. ^{b} OF is the Na/T occupancy factor in the indicated position. T indicates the trivalent cations Y(Lu) or Y(Lu) and Yb.

Table 4. Selected Bond Lengths (Å) for $\text{NaT}_{1-x}\text{Yb}_x(\text{WO}_4)_2$, T = Y or Lu, Crystals

	NaYW	$\text{NaY}_{0.9}\text{Yb}_{0.1}\text{W}$	NaLuW	$\text{NaLu}_{0.9}\text{Yb}_{0.1}\text{W}$	$\text{NaLu}_{0.5}\text{Yb}_{0.5}\text{W}$
Na(1)/T(1)−O(1)×4	2.438(15)	2.45(2)	2.408(13)	2.41(2)	2.406(13)
Na(1)/T(1)−O(2)×4	2.414(14)	2.46(2)	2.395(15)	2.38(2)	2.392(13)
Na(2)/T(2)−O(1)×4	2.453(18)	2.40(2)	2.441(16)	2.41(2)	2.423(15)
Na(2)/T(2)−O(2)×4	2.420(17)	2.42(3)	2.405(15)	2.39(3)	2.411(15)
W(1)−O(1)×4	1.756(17)	1.80(2)	1.762(16)	1.78(3)	1.769(15)
W(2)−O(2)×4	1.804(15)	1.76(3)	1.799(16)	1.82(3)	1.797(14)
Na/T(1)−Na/T(2)	3.8350(5)	3.8348(8)	3.8074(3)	3.8071(7)	3.8034(4)
Na/T(1)−W(1)	3.8350(5)	3.8348(8)	3.8074(3)	3.8071(7)	3.8034(4)
Na/T(1)−W(2)	3.6779(3)	3.6784(6)	3.6552(2)	3.6559(8)	3.6568(5)
Na/T(2)−W(1)	3.6779(3)	3.6784(6)	3.6552(2)	3.6559(8)	3.6568(5)
Na/T(2)−W(2)	3.8350(5)	3.8348(8)	3.8074(3)	3.8071(7)	3.8034(4)

melting point for TSSG crystals is related to the increased flux concentration in the $\text{NaLu}_{1-x}\text{Yb}_x(\text{WO}_4)_2/\text{Na}_2\text{W}_2\text{O}_7$ mixture. The growth temperature used in the TSSG method is about 300 K lower than that required for the Cz growth.

Table 1 summarizes the metal compositions of each crystal as determined by XRFS along with some information on the growth conditions. According to these results, Cz-grown crystals are Na^+ deficient, which is compensated by the incorporation of an excess of Y^{3+} and Yb^{3+}. This deficiency is not observed in TSSG crystals. These compositional differences must be related to the different crystal growth temperatures, which influence Na^+ and W^{6+} volatilities, as well as to the incorporation into the crystal of these constituents from the flux. In fact, the materials that evaporated during the growth resolidify on the ceramic tube wall around the crucible and in the pulling rod. Compounds formed after resolidification of vapors from the melt were identified as sodium tungsten bronzes, i.e., phases resulting from the intercalation of Na in WO_3, Na_xWO_3, $x < 1$.[33]

Crystalline Structure. The two tetragonal space groups, namely $I4_1/a$ and $I\bar{4}$, proposed for $\text{NaT}(\text{WO}_4)_2$ involve structural disorder. Na^+ and T^{3+} (Y, Lu, or Yb) ions randomly share either an unique 4b crystallographic site, with

(33) Slade, R. C. T.; West, B. C.; Hall, G. P. *Solis State Ionics* **1989**, *32/33*, 154.

S_4 point symmetry, for SG $I4_1/a$, or two independent, also S_4, 2b and 2d sites in the SG $I\bar{4}$. In the latter case, although T^{3+} has 8-fold oxygen coordination in both sites, T−O distances and O−T−O angles are different for each site. Furthermore, multiple short-range Na^+ and T^{3+} environments in the first cationic shell around each Yb^{3+} also generate a distribution of crystal fields on Yb^{3+}. Since the magnitude of the total Yb^{3+} bandwidth is determined by a convolution of the lineshapes due to the local environments around the different point sites, the predicted existence of more than one Yb^{3+} point site in $I\bar{4}$ will enhance the spectral broadening of Yb^{3+}, and consequently the related laser tunability. Therefore, determining the controversial crystalline structure is relevant for the correct interpretation of the observed Yb^{3+} optical properties.

Our initial analyses of single-crystal X-ray data for pure and Yb-doped $\text{NaT}_{1-x}\text{Yb}_x\text{W}$, T = Y, Lu, showed the presence of a certain number of systematic absence exceptions, for the a plane, (h −h 0), $h \neq 2n$ (the SG $I4_1$ will be still possible) and for the 4_1 axis, (0 0 l), l even but $l \neq 4n$, with intensity $I > 3\sigma(F)$, that is well above the $I > 2\sigma(F)$ threshold for the Bragg reflections considered in the current refinements. The observation of both types of systematic absence exceptions, see Table 2, reveals undoubtedly the distortion from the centrosymmetric SG $I4_1/a$ to the noncen-
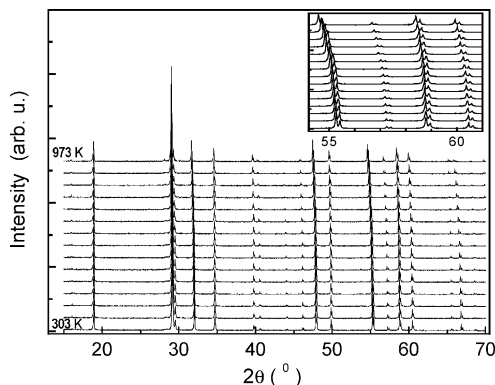
Figure 2. Thermal evolution of collected XRPD patterns for ground NaLu$_{0.9}$Yb$_{0.1}$W crystal. The inset shows the detail of some well-resolved reflections.
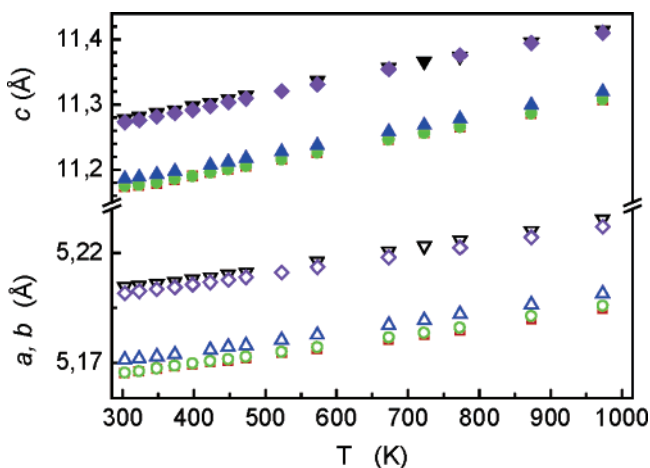

Figure 3. Thermal evolution of *a* (open symbols) and *c* (full symbols) lattice parameters for the $I\bar{4}$ phase of Na-double tungstates: ▽, ▼ NaYW; ◇, ◆NaY$_{0.9}$Yb$_{0.1}$W; □, ■ NaLuW; ○, ● NaLu$_{0.9}$Yb$_{0.1}$W; △, ▲ NaLu$_{0.5}$-Yb$_{0.5}$W.

Figure 4. Thermal evolution of *c/a* ratio for the $I\bar{4}$ phase of Na-double tungstates: ▼ NaYW; ◆ NaY$_{0.9}$Yb$_{0.1}$W; ■ NaLuW; ● NaLu$_{0.9}$Yb$_{0.1}$W; ▲ NaLu$_{0.5}$Yb$_{0.5}$W.

Figure 5. Evolution with T of the thermal expansion coefficients (K^{-1}) along the *a*-axis, α_1 (open symbols), and along the *c*-axis, α_3 (full symbols), of the tetragonal $I\bar{4}$ phase of Na-double tungstates: ▽, ▼ NaYW; ◇, ◆NaY$_{0.9}$Yb$_{0.1}$W; □, ■ NaLuW; ○, ● NaLu$_{0.9}$Yb$_{0.1}$W; △, ▲ NaLu$_{0.5}$Yb$_{0.5}$W.

trosymetric SG $I\bar{4}$. The following crystal structure refinements, conducted to adequately low final discrepancy *R* factors, provide the atomic coordinates, the distribution of the alkaline Na$^+$ and T^{3+}, Y^{3+}/Yb^{3+}/Lu^{3+} cations in the two independent S_4 2*b* and 2*d* point sites, that is, the occupancy factors (OFs) over these two sites, and positive anisotropic thermal displacements for all atoms. Results from the refinement of the OFs for W sites were considered when they yielded significantly lower *R* factors. Table 2 gives the details on X-ray data collection and structure refinements. Atomic coordinates, OFs for Na and T shared crystal sites as well as for W positions appear in Table 3, and selected bond distances are in Table 4.

Compositions derived from the single-crystal XRD refinements indicate that TSSG NaLu$_{1-x}$Yb$_x$W crystals are nearly stoichiometric, whereas for the Cz grown NaY$_{1-x}$Yb$_x$W crystals they show Na$^+$ deficiency and charge compensation by incorporation of a excess of T^{3+} (either Y alone or Y and Yb), in agreement with XRFS analysis. The W^{6+} deficiency reported for some of these crystals is within the experimental error limit, and therefore is less significant. Similar features, small and very small Na$^+$ and W^{6+} deficiencies, respectively, and excess of T^{3+}, have also been observed for other Cz-grown Na-based crystals, NaGd$_{1-x}$Yb$_x$W crystals.[6]

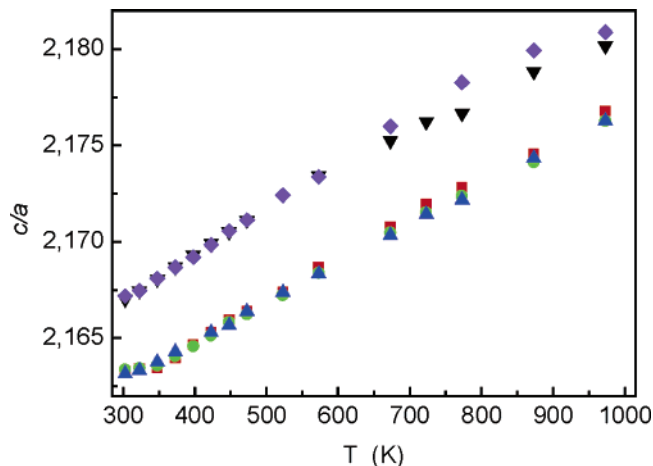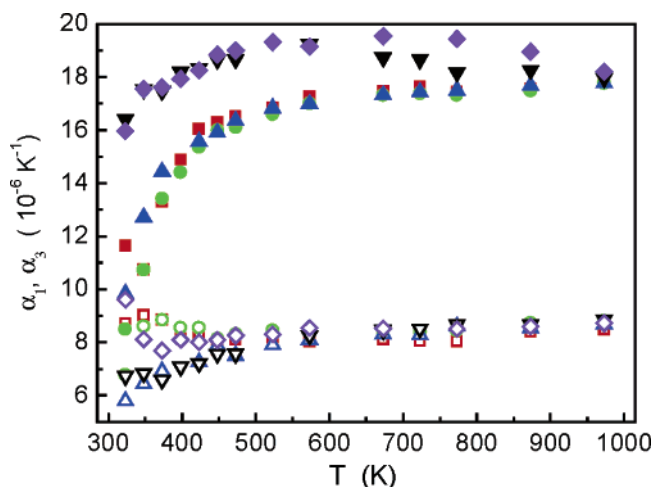The distribution of Na$^+$ and T^{3+} (Y, Yb, Lu) cations sharing the 2*b* and 2*d* point sites, a crystallographic characteristic connected to some spectroscopic properties,[6] is remarkably different in Y- or Lu-containing crystals, see OFs in Table 3. The closer to random OF data for NaLu$_{1-x}$Yb$_x$W indicate more disordered Yb^{3+} environments in such crystals. The results of NaLu$_{0.5}$Yb$_{0.5}$W reveal relative intensities of (0 0 *l*), *l* ≠ 4*n* and (*h* $\bar{h}$ 0), *h* ≠ 2*n*, reflections stronger than those observed in undoped and weakly Yb-doped NaLuW crystals. However, the cationic order derived from the OF of 2*d* and 2*b* sites only increases slightly with regard to lower Yb-content.

The DT crystalline structure corresponding to the SG $I\bar{4}$ contains two kinds of WO$_4$ tetrahedra and (Na$^+$/T^{3+})O$_8$ distorted square antiprisms, see Figure 1c,d. It can be described as consisting of parallel chains of alternate WO$_4$ and (Na$^+$/T^{3+})O$_8$, which are sharing one vertex along the *a*- and *b*- directions, of only one type in each row, and in the *c* direction two different (Na$^+$/T^{3+})O$_8$ polyhedra from two consecutive chains are linked through a common edge, forming dimeric (Na$^+$/T^{3+})$_2$O$_{14}$ units (see the detailed view in Figure 1d) in such way that each (Na$^+$/T^{3+})O$_8$ shares four
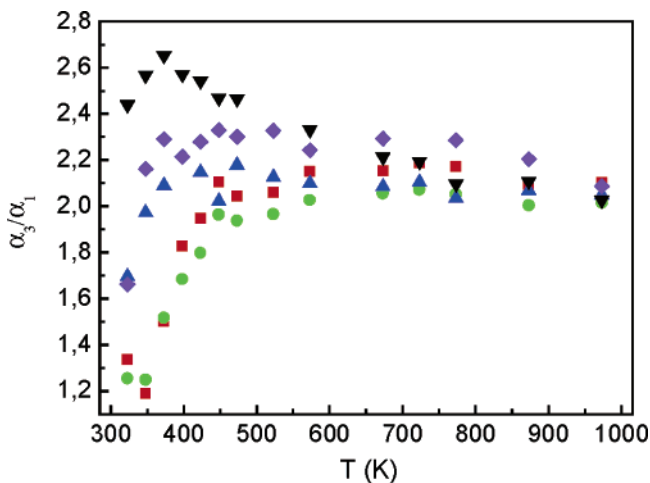
Figure 6. Thermal evolution of the α_3/α_1 ratio for the $I\bar{4}$ phase of Na-double tungstates: ▼ NaYW; ♦ NaY$_{0.9}$Yb$_{0.1}$W; ■ NaLuW; ● NaLu$_{0.9}$Yb$_{0.1}$W; ▲ NaLu$_{0.5}$Yb$_{0.5}$W.
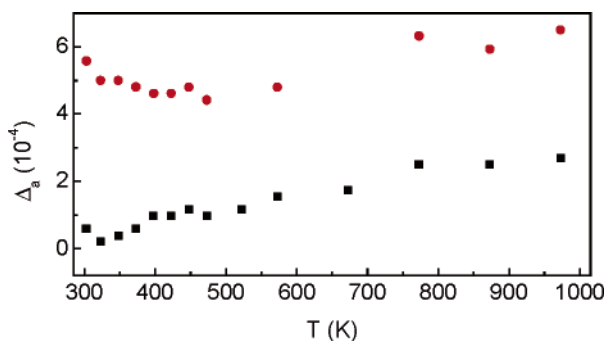

Figure 7. Yb-doped layer/optically inert substrate *a* unit cell lattice mismatch Δ_a for ■ NaLu$_{0.9}$Yb$_{0.1}$W/NaLuW and ● NaY$_{0.9}$Yb$_{0.1}$W/NaYW.

of its edges with other four $(Na^+/T^{3+})O_8$ polyhedra, and the eight vertexes with WO$_4$ tetrahedra.

Thermal Properties: Thermal Expansion Tensor. XRPD patterns for the five samples indicate that the crystal symmetry remains the same in the whole range of measured temperatures. As an example, Figure 2 shows the collected XRPD scans for NaLu$_{0.9}$Yb$_{0.1}$W. For the five studied compositions the variation of *a* and *c* unit cell parameters as a function of the temperature is depicted in Figure 3. It can be seen that in all cases they increase monotonically when the temperature is getting higher. Figure 4 shows the thermal evolution of the *c/a* ratio. Lattice parameters for the five samples at temperatures in the 303–973 K range are included in Table A of the Supporting Information.

The cell strain d*U* due to a temperature variation d*T* is expressed by a second-rank tensor $dU_{ij} = \alpha_{ij}\,dT$, where α_{ij} (K^{-1}) are the coefficients of the thermal expansion tensor. At a given temperature, the knowledge of the principal α_{ij} coefficients and of the direction of the principal axes of the tensor allows the determination of the strongest and the weakest directions of the corresponding intermolecular interactions. For tetragonal crystals there are only two independent principal thermal expansion components, $\alpha_1 \equiv \alpha_2$ (along the *a*- or *b*-axis) and α_3 (along the *c*-axis). Therefore, the thermal expansion tensors of the studied Na-based DT can be determined from the thermal changes in lattice parameters shown in Figure 3, by evaluating the relationship between the expansion ratio of the corresponding

Table 5. Average Thermal Expansion Coefficients α_1 and α_3 in the Temperature Range 500–973 K for Tetragonal $I\bar{4}$ Na-Double Tungstates

	NaYW	NaY$_{0.9}$Yb$_{0.1}$W	NaLuW	NaLu$_{0.9}$Yb$_{0.1}$W	NaLu$_{0.5}$Yb$_{0.5}$W
α_1 (10^{-6} K^{-1})	8.4 (2)	8.5(2)	8.2(2)	8.5(2)	8.4(2)
α_3 (10^{-6} K^{-1})	18.5(4)	19.1(4)	17.3(4)	17.3(4)	17.4(3)
α_3/α_1	2.2	2.3	2.1	2.0	2.1

a- or *c*-parameters and the temperature: $\alpha(T) = (\Delta p(T))/(p_{RT} \times \Delta T)$, where p_{RT} is the unit cell parameter at room temperature (in our experiments 303 K), $\Delta p(T) = p(T) - p_{RT}$ is the cell parameter change for a given temperature *T*, and ΔT is the temperature increase above room temperature.

For the studied Na-based DTs the curves corresponding to the evolution with *T* of the thermal expansion coefficients α_1 and α_3 along *a* and *c* crystal axes, respectively, are shown in Figure 5, and the α_3/α_1 ratio in Figure 6. A significant change in these coefficients is observed in the 303–500 K range, particularly in α_3 for NaLu-based DTs, but above 500 K their values become nearly constant. Table 5 gives the average α_1 and α_3 values, calculated for the 500–973 K interval. In all examined crystals the expansion coefficient in the direction of the *c*-axis is about 2 times larger than the corresponding value along *a*; that is, the thermal expansion is strongly anisotropic.

This anisotropic behavior can be related to the different nature and arrangement of the coordination polyhedra (Na/T)O$_8$ and WO$_4$ in [100] and [001] directions of the $I\bar{4}$ crystal structure. Due to the strong covalent character of W–O bonds in WO$_4$, with distances of $\approx$1.8 Å, these tetrahedra are considered the "hard" or rigid units in the scheelite structure,[34] and they remain nearly unchanged with the increase of temperature. As a consequence, the thermal expansion of the studied Na-based DTs will be mainly governed by the expansion of the Na/TO$_8$ polyhedra, whose Na/T–O bonds are considerably larger, $\approx$2.4 Å. The presence of rigid WO$_4$ tetrahedra alternated with Na/TO$_8$ along *a*- or *b*-axes, see Figure 1c,d, restrains the thermal expansion of the crystal, and confers stiffness to the structure in these directions. The *c*-axis has a higher expansion due to the presence of dimeric (Na/T)$_2$O$_{14}$ units along this direction. Furthermore, at room-temperature typical Na/T–W distances along *a*- or *b*-directions are shorter, $\approx$3.66 Å, than in the perpendicular direction, $\approx$3.81 Å, see Table 4. Thus, the expected higher thermal expansion of Na/T–W bonds along *c* with regard to the corresponding value for these bonds in *a*- or *b*-directions will also contribute to larger thermal expansion coefficients in the *c*-direction.

The inspection of results of Figures 5 and 6 and Table 5 indicates that the thermal expansion of the NaYW unit cell is more anisotropic than for NaLuW, especially below 600 K. In fact, whereas differences between α_1 values are small in both hosts and even can be considered within the measurement error, α_3 is clearly higher for NaYW. The weakening of the interatomic interactions along *c* as consequence of the larger Na/Y–O bonds and the increase in the intermetallic distance Na/Y–Na/Y, see Table 4, could

(34) Hazen, R. M.; Finger, L. W.; Mariathasan, J. W. E. *J. Phys. Chem. Solids* **1985**, *46*, 253.

Table 6. Comparison of Thermal Expansion Coefficients α_1 and α_3 for Several Tetragonal Na-Double Tungstates[a]

	NaYW:Nd	NaYW:Yb	NaGdW:Tm	NaGdW:Yb	NaTbW	NaTbW	NaYbW	NaYbW
technique	DIL	DIL	DIL	DIL	XRD	XRD	XRD	XRD
T (K)	293–573	303–873	673–1273	303–873	303	583	303	743
α_1 (α_2) (10^{-6} K^{-1})	3.5	13.5 (12.7)	7.89	6.70	6.49	13.65	3.63	12.59
α_3 (10^{-6} K^{-1})	17.7	22.9	16.0	16.27	9.70	16.19	7.02	17.47
α_3/α_1	5.1	1.7 (1.8)	2.0	2.4	1.5	1.2	1.9	1.4
growth method	Cz	Cz	Cz	Cz	N.A.	N.A.	N.A.	N.A.
ref	42	38	43	38	44	45	21	45

[a] The experimental technique used was dilatometry (DIL) or X-ray Diffraction (XRD). To derive α_1 and α_3, the temperature range of measurement and the method of preparation of crystals are also indicated.

contribute to its higher expansion along the *c*-axis. On the other hand, the progressive incorporation of Yb in NaLuW does not suppose noticeable changes in the thermal anisotropy of the crystal, which moreover is expected taking into account the similar ionic radii size for Lu^{3+} and Yb^{3+}. On the contrary, even the doping with [Yb]$_{MELT}$ = 10 mol % in NYW definitely involves larger α_3 values, and thus higher thermal anisotropy of the crystal.

The comparison of the current results with those of other tetragonal scheelite-type single tungstates CaWO$_4$,[35,36] SrWO$_4$,[37,38] or BaWO$_4$,[39,40,41] or even double tungstates, Nd-doped NaY(WO$_4$)$_2$,[42] Yb-doped NaY(WO$_4$)$_2$,[38] Tm-doped NaGd(WO$_4$)$_2$,[43] Yb-doped NaGd(WO$_4$)$_2$,[38] NaTb(WO$_4$)$_2$,[44,45] NaYb(WO$_4$)$_2$[21,45] or KLa(WO$_4$)$_2$,[45] is not straightforward because of the differences in experimental techniques and studied temperature ranges. With regards to Na-based DT, for which corresponding data are collected in Table 6, the thermal expansion of all of them is anisotropic. Most of the average α_3 values reported lie in a relatively short range α_3 = 16–23 × 10^{-6} K^{-1}, similar to the current results for NaT$_{1-x}$Yb$_x$W (T = Y or Lu) crystals. Larger differences are found for α_1, from 3.5 × 10^{-6} K^{-1} for Nd-doped NaYW, up to 13.65 × 10^{-6} K^{-1} for NaTbW. Anyway, if the comparison of our data is restricted to data for Yb-doped NaYW or NaGdW, both obtained by dilatometry in the same range of temperature,[38] it seems reasonable to attribute the observed increase in the thermal expansion anisotropy of the latter to the larger size of the Gd^{3+} cation.

From presented results on undoped and Yb-doped NaY$_{1-x}$Yb$_x$W or NaLu$_{1-x}$Yb$_x$W crystals, the smallest density of light scattering defects at the laser layer/optically inert substrate interface is expected for NaLu$_{1-x}$Yb$_x$W/NaLuW composites. Nevertheless, even for these favorable combina-tions, some lattice mismatch originated by the Yb-doping is still present. These aspects as well as an approach to avoid this mismatch are developed in the following subsection.

Tailoring Lattice Matched Yb-Doped Double Tungstate Composites: Effects of Temperature and Substrate Composition. From the unit cell parameters collected in Figure 3, the Yb-doped layer/optically inert substrate lattice mismatch can be calculated for a specific temperature. The lattice mismatch can be defined as $\Delta = |p_l - p_s|/p_s$, where p_l and p_s are the unit cell parameters of the Yb-doped laser layer and the optically inert substrate, respectively. It is clear that if *c*-cut tetragonal DT substrates were chosen for epitaxial growth of Yb-doped layers it will be possible to avoid the in-plane anisotropy; thus, we will consider first the lattice mismatch for the *a* unit cell parameter, Δ_a. Regarding the thermal behavior, the comparison of Δ_a for different NaT$_{1-x}$Yb$_x$W/NaTW composites, with the same level of Yb-doping, is an indication of their relative steadiness upon cooling and during optical pumping cycles. From crystal data for x = 0.10, NaLu$_{1-x}$Yb$_x$W/NaLuW composites present in the whole temperature range (growth temperature to 300 K) lower lattice mismatch than any other simple combination of tetragonal Na-based DTs. Even in comparison to the close size NaY$_{1-x}$Yb$_x$W/NaYW ones Δ_a is about 2.5 times lesser than for the latter, see Figure 7.

Although small, the NaLu$_{1-x}$Yb$_x$W/NaLuW lattice mis-match is different from zero. It would be desirable to vanish the layer/substrate lattice mismatch derived from the Yb incorporation. While for NaLu$_{1-x}$Yb$_x$W the lattice parameters increase linearly with the Yb-doping, see Table 2, similar linear variation can be expected in the substrate by mixing Lu and T = Y, Gd, or La, leading in all cases to optically inert substrates. This linear variation of the lattice parameters of mixed DTs has been confirmed with polycrystalline samples. Lattice parameters for the three series NaLu$_{1-x}$T$_x$W, T = La (x = 0.03, 0.06, 0.10, 0.15), Gd or Y (x = 0.05, 0.10, 0.15, 0.20, 0.25), are included in Table B of the Supporting Information, and the results are collected in Figure 8, which shows the evolution of the *a*-and *c*-parameters for optically inert NaLu$_{1-x}$T$_x$W, T = Y, La, Gd, as well as for Yb-doped NaLuW, with the Lu content. These plots provide a graphical method to determine the substrate composition with Δ_a= 0 for a given Yb concentra-tion in the layer. For instance, for a NaLu$_{0.5}$Yb$_{0.5}$(WO$_4$)$_2$ layer, a = 5.1715 Å, the suitable substrate with could be any NaLu$_{1-x}$T$_x$(WO$_4$)$_2$ with T$_x$ = Y$_{0.06}$, Gd$_{0.027}$, or La$_{0.011}$, see Figure 8, top.

A composite with Δ_a = 0 from a *c*-cut tetragonal DT would be very suitable to produce a laser waveguide

(35) Bayer, G. *J. Less-Common Met.* **1971**, *26*, 255.
(36) Achary, S. N.; Patwe, S. J.; Mathews, M. D.; Tyagi, A. K. *J.Phys. Chem. Solids* **2006**, *67*, 774.
(37) Ling, Z. C.; Xia, H. R.; Ran, D. G.; Liu, F. Q.; Sun, S. Q.; Fan, J. D.; Zhang, H. J.; Wang, J. Y.; Yu, L. L. *Chem. Phys. Lett.* **2006**, *426*, 85.
(38) Fan, J.; Zhang, H.; Wang, J.; Ling, Z.; Xia, H.; Chen, X.; Yu, Y.; Lu, Q.; Jiang, M. *J. Phys. D: Appl. Phys.* **2006**, *39*, 1034.
(39) Ge, W.; Zhang, H.; Wang, J.; Liu, J.; Li, H.; Cheng, X.; Xu, H.; Xu, X.; Hu, X.; Jiang, M. *J. Cryst. Growth* **2005**, *276*, 208.
(40) Chauhan, A. K. *J. Cryst. Growth* **2003**, *254*, 418.
(41) Ge, W. W.; Zhang, H. J.; Wang, J. Y.; Liu, J. H.; Xu, X. G.; Hu, X. B.; Jiang, M. H.; Ran, D. G.; Sun, S. Q.; Xia, H. R.; Boughton, R. I. *J. Appl. Phys.* **2005**, *98*, 013542.
(42) Cheng, Z.; Zhang, S.; Fu, K.; Liu, J.; Chen, H. *Jpn. J. Appl. Phys.* **2001**, *40*, 4038.
(43) Wang, H.; Jia, G.; Yang, F.; Wei, Y.; You, Z.; Wang, Y.; Li, J.; Zhu, Z.; Lu, X.; Tu, C. *Appl. Phys. B* **2006**, *83*, 579.
(44) Sadanandam, J.; Suryanarayana, S. V. *Natl. Acad. Sci. Lett. (India)* **1979**, *2*, 37.
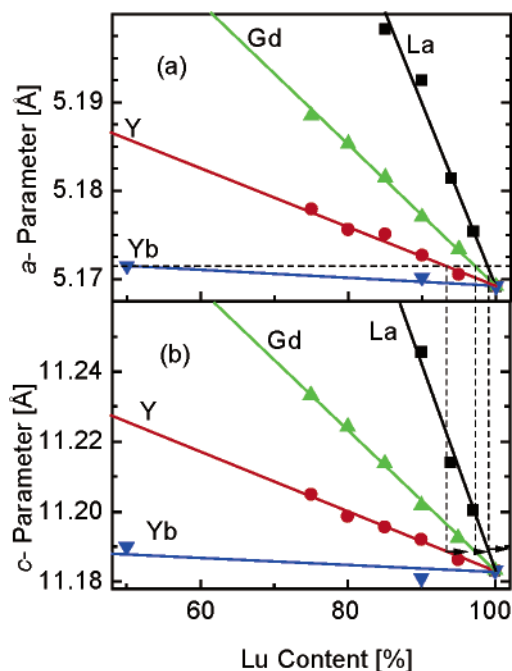(45) Suryanarayana, S. V.; Sadanandam, J. *J. Mater. Sci. Lett.* **1984**, *3*, 408.

Figure 8. Evolution of the a (top) and c (bottom) lattice parameters for NaLu$_{1-x}$T$_x$W, T = Y, La, Gd, and Yb. The dashed lines indicate the graphical method for the calculation of the composition of lattice matched substrates.

structure, allowing the selection of σ or π excitation configurations. However, if this composite was used in the thin disk geometry, the pump beam direction would be close to the c-axis, and therefore, the excitation would correspond to a α ($\approx\sigma$) spectrum. For the particular case of NaLu$_{1-x}$Yb$_x$W, the σ and π gain cross sections and laser tuning properties are very similar,[15] but in other NaT$_{1-x}$Yb$_x$W crystals the laser performance in π configuration is better than in the σ one.[6,12,13] To optimize the latter configuration, composites on a-cut substrates would be required. Let us then examine the relationship between the lattice mismatches of both crystal axes.

For a given Yb composition of the layer, after choosing substrate compositions corresponding to $\Delta_a = 0$, the c-axis lattice mismatches Δ_c can be obtained with the help of the graphical method sketched in Figure 8, bottom. Laser action in bulk crystals has been optimized for $x \approx 0.1$.[6,12,15,17] For this composition of the Yb-doped layer Δ_c for the NaLuW

substrate is 6.5×10^{-5}, and for NaLu$_{1-x}$T$_x$W substrates it changes to 7.0×10^{-5}, 4.9×10^{-5}, and 3.6×10^{-5} for T = La, Gd, and Y, respectively. Therefore, the lowest lattice mismatches are found in NaLu$_{1-x}$Yb$_x$W/NaLu$_{1-x}$Y$_x$W composites.

Conclusions

NaT$_{1-x}$Yb$_x$W, T = Y or Lu, crystals have been grown free of macrodefects by the Cz (T = Y) or TSSG (T = Lu) methods. Only the noncentrosymmetric tetragonal space group $I\bar{4}$ accounts for all reflections observed in their single-crystal X-ray diffraction analysis. In this symmetry, there are two sites, 2b and 2d, shared by Na$^+$ and T^{3+} (Y^{3+}, Yb^{3+}, Lu^{3+}) cations, with specific occupancy factors. The lowest departure from the random distribution is found in NaLu$_{1-x}$Yb$_x$W crystals. Noticeable differences have also been observed in the composition of Cz and TSSG crystals, which are Na-deficient and stoichiometric materials, respectively.

The thermal expansion in all the title crystals is strongly anisotropic, with expansion coefficients in the direction of the c-axis typically 2 times larger than the corresponding values along the a-axis. This thermal anisotropy is minimized in NaLu$_{1-x}$Yb$_x$W crystals. Moreover, NaLu$_{1-x}$Yb$_x$W/NaLuW composites are the most stable upon thermal changes.

Room temperature a-axis zero-lattice mismatch between the Yb-doped DT layer and the optically inert DT substrate can be obtained by substitution of Lu by small amounts of Y, Gd, or La in the substrate. Between these possibilities, the Y substitution is the most favorable to simultaneously minimize the c-axis lattice mismatch.

Supporting Information Available: Tables of unit cell parameters of tetragonal double tungstates (PDF). This material is available free of charge via the Internet at http://pubs.acs.org.

CM070237V